

11-1995


Image Restoration of Dispersion-Degraded Images from a Liquid-Crystal Beam Steerer

Ronald J. Broessel
University of Dayton

Vince Dominic
University of Dayton

Russell C. Hardie
University of Dayton, rhardie1@udayton.edu

Follow this and additional works at: https://ecommons.udayton.edu/ece_fac_pub

 Part of the [Optics Commons](#), and the [Signal Processing Commons](#)

eCommons Citation

Broessel, Ronald J.; Dominic, Vince; and Hardie, Russell C., "Image Restoration of Dispersion-Degraded Images from a Liquid-Crystal Beam Steerer" (1995). *Electrical and Computer Engineering Faculty Publications*. 6.
https://ecommons.udayton.edu/ece_fac_pub/6

This Article is brought to you for free and open access by the Department of Electrical and Computer Engineering at eCommons. It has been accepted for inclusion in Electrical and Computer Engineering Faculty Publications by an authorized administrator of eCommons. For more information, please contact frice1@udayton.edu, mschlangen1@udayton.edu.

Image restoration of dispersion-degraded images from a liquid-crystal beam steerer

Ronald J. Broessel
 Vince Dominic
 Russell C. Hardie
 University of Dayton
 Center for Electro-Optics
 Dayton, Ohio 45469-0245
 E-mail: vdominic@enr.dayton.edu

Abstract. Liquid-crystal arrays represents one of the first practical technologies capable of steering light by electronic control only. We use such a device to steer the field of view of a broadband imaging sensor. Unfortunately, dispersion degrades the image quality by smearing out details in the image and by introducing multiple diffraction orders (echoes) at the detector plane. We present a method to compensate for these unwanted effects and thus restore the broadband images obtained with the beam steerer. We use the beam-propagation method to find the wavelength-dependent impulse response, from which we determine the appropriate Wiener filter. When training data are available, we improve the filter with the adaptive least mean square algorithm. We present restored images that demonstrate the capabilities of this technique.

Subject terms: optical remote sensing and image processing; liquid crystals; beam steering; imaging; adaptive signal processing.

Optical Engineering 34(11), 3138–3145 (November 1995).

1 Introduction

Optical beam steering has many interesting industrial and military applications, including laser radar, laser beam scanning, pointing stabilization, and microscanning.¹⁻⁴ Mechanical beam-steering technology (based on mirrors) allows rapid, large-angle deflection and scanning of optical beams, but fails to meet high-resolution performance requirements.¹ Liquid-crystal beam-steering devices represent the first practical technology capable of providing accurate, agile, and inertialess beam steering using electronic control only. Such devices eliminate the need for bulky, complex mechanical systems, thus reducing weight and increasing reliability. The liquid-crystal beam steerer borrows microwave-radar concepts to implement random-access, nonmechanical beam steering with optical phased arrays.⁵

If a beam-steering device provides a linearly increasing optical phase delay (OPD) across its aperture, it will steer light just like a prism. The outgoing beam tilts because its phase front is advanced on one side of the aperture and delayed on the opposite side. In a liquid-crystal beam steerer, the applied electric field realigns birefringent liquid crystals and so controls the OPD. By altering the voltage applied to

a series of electrodes, we manipulate the spatial variation of the OPD. Monotonically increasing the voltages across the device aperture creates a phase profile resembling that of a prism. Instead of the thickness T varying linearly across the aperture (direction x) as

$$\text{prism: } \text{OPD} = \frac{2\pi}{\lambda} nT(x) , \quad (1)$$

the differential refractive index $\delta n(x) = n_e - n(x)$ varies linearly (n_e is the extraordinary refractive index):

$$\text{beam steerer: } \text{OPD} = \frac{2\pi}{\lambda} \delta n(x) T . \quad (2)$$

The differential index δn varies nonlinearly with the control voltage and is at most equal to the birefringence Δn of the liquid crystal (≈ 0.2 in the midvisible for E7).⁶

A prislime phase profile steers all the incident energy at the design wavelength λ_{design} to the desired angle. However, as the wavelength shifts away from λ_{design} , the steering angle changes according to

$$\text{prism: } \theta_{\lambda_{\text{probe}}} = \theta_{\lambda_{\text{design}}} \frac{\Delta n(\lambda_{\text{probe}})}{\Delta n(\lambda_{\text{design}})} \quad (3)$$

Paper RS-012 received Mar. 31, 1995; revised manuscript received June 1, 1995; accepted for publication June 19, 1995.
 © 1995 Society of Photo-Optical Instrumentation Engineers. 0091-3286/95/\$6.00.

for small steering angles. Material dispersion alters the steering angle for wavelengths other than λ_{design} .

Unfortunately, devices with prismatic OPD profiles cannot be used, because they are too thick and therefore too slow. The liquid-crystal realignment time is proportional to the square of the layer thickness.¹ A linearly increasing phase ramp across a 4-cm device aperture requires an $\approx 112\text{-}\mu\text{m}$ -thick layer to steer to 0.024 deg. Such a device will be impractically slow for laser radar applications.¹⁻³ The thickness of the liquid-crystal layer is greatly reduced by subtracting out regions of 2π phase from the original profile. Multiples of 2π are indistinguishable and do not affect the propagation of the beam at the design wavelength. The new phase profile resembles a blazed diffraction grating, as shown in Fig. 1(c). This phase-reset profile reduces the thickness of the crystal layer to $\approx 7\text{ }\mu\text{m}$ and gives fast switching times (4 to 5 ms). We use these fast devices to rapidly steer the field of view of a broadband optical sensor. Unfortunately, the phase structure described above significantly degrades broadband images.

The grating nature of the phase profile introduces trouble when steering broadband radiation because the 2π phase resets are correct at only one wavelength.¹⁻³ Wavelengths other than λ_{design} have an incorrect phase shift ($\neq 2\pi$) at the resets. The resultant grating dispersion produces a smeared and echoed version of the original scene at the detector plane: we have both multiple grating orders [m in Eq. (4)] and wavelength-dependent smearing [λ in Eq. (4)]:

$$\sin\theta = m \frac{\lambda}{\Lambda}, \quad (4)$$

where Λ is the phase ramp reset distance. Restoration of the image is difficult due to the combination of degradation mechanisms.

2 Restoration Algorithms

Image restoration is the process of minimizing the known degradations in an image.⁷ For the beam-steering apparatus the worst degradations are blurring, caused by material and grating dispersion, and echoing, caused by multiple diffraction orders. To undo these image degradations, we first developed a beam-propagation model (BPM) that provides a good estimate of the beam-steerer impulse response as a function of wavelength. Based on this, we then find the Wiener filter for image restoration. The Wiener filter⁷ gives the best mean-square estimate of the original object and can accommodate the presence of additive noise in images. Unfortunately, we must know or estimate the noise and signal statistics, because the optimal Wiener filter requires the noise-to-signal power spectral density ratio. This information is often difficult to obtain *a priori*, and we therefore resort to a spectrally flat noise-to-signal ratio in our Wiener filter. In addition, when we have the luxury of "training data" for the device (knowledge of the steered and unsteered images), then we use a least mean square (LMS) adaptive algorithm to improve the image restoration filter. The LMS algorithm is the simplest and most widely used algorithm for adjusting the weights in a linear adaptive system.⁸ Our application makes efficient use of a train of standard algorithms: BPM \rightarrow Wiener filter \rightarrow LMS, as summarized in Table 1.

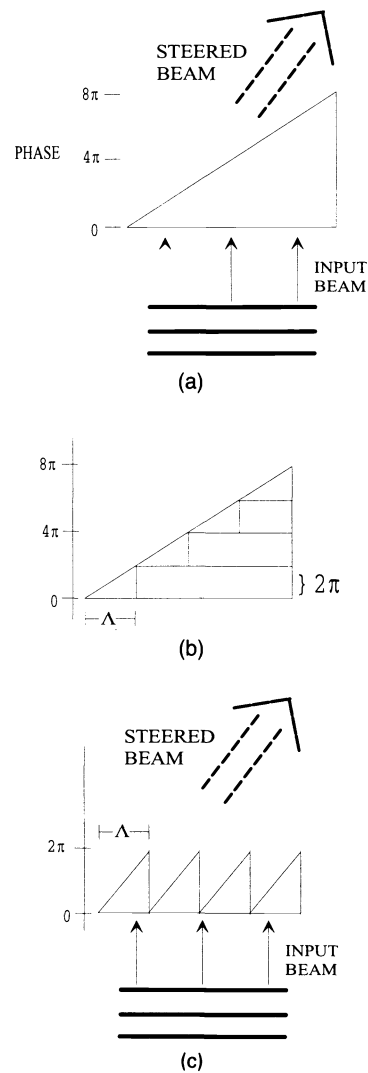


Fig. 1 Phase profile of beam-steering device: (a) full prismatic phase across aperture, (b) decomposition of phase by removal of 2π phase steps, (c) resulting phase ramps.

We describe each algorithm before presenting narrow- and broadband image restoration results.

2.1 Beam-Propagation Method

One of the most robust and efficient methods for analyzing diffraction problems is the well-known BPM.⁹⁻¹¹ The BPM is quite general and can model optical beam propagation through scattering and distorting media such as the atmosphere, optical fibers, volume holographic elements, grating lenses, spatial light modulators, etc. The BPM simplifies the actual propagation problem by splitting it into two parts: propagation and modulation. First we decompose the optical beam into its spatial frequencies,¹² and then we propagate

Table 1 Summary of the image resolution algorithm.

- | |
|---|
| <ol style="list-style-type: none"> 1) Find the BPM model impulse response 2) Estimate the signal statistics and calculate the Wiener filter 3) If training data exists, refine the filter with the LMS algorithm |
|---|

them by adjusting their relative phases. For a beam traveling in the z direction, the slowly varying envelope function $A(x, z)$ is written as

$$A(x, z) = \sum_{\ell = NX/2}^{NX/2 - 1} \mathcal{A}_\ell(z) \exp\left(\frac{i2\pi\ell x}{X_{\max}}\right), \quad (5)$$

where we assume that the slowly varying envelope was sampled at NX points over a spatial domain of extent X_{\max} and that only one transverse coordinate (x) is needed to describe the problem. This is equivalent to decomposing the amplitude into plane waves traveling at angles

$$\theta_\ell = \ell \frac{\lambda}{X_{\max}}. \quad (6)$$

The spatial frequencies propagate according to

$$\mathcal{A}_\ell(z + \Delta z) = \mathcal{A}_\ell(z) \exp\left(i\pi \frac{\Delta z}{\lambda} \theta_\ell^2\right). \quad (7)$$

In the *absence* of modulation effects we simply Fourier-transform the slowly varying amplitude function at its current position z , multiply the transform by a complex phase factor, and then transform back to get the amplitude at the new plane $z + \Delta z$. Each plane-wave component travels at a slightly different angle [Eq. (6)], so that after traversing a slice of material Δz thick the angular components accumulate different optical phases [Eq. (7)]. The BPM is computationally efficient because it involves only two FFT operations and one complex multiplication per slice.

We handle the modulation aspect of the problem by imagining that we slice our medium into many thin pieces. If the slices are thin enough, then the beam shape will not change much in crossing them. We allow the beam to cross the first half of our slice without modulation effects, using Eq. (7). Over the next half slice we ignore the diffraction problem and allow only modulation effects via the following simple multiplication:

$$A(x, z + \Delta z) = \exp\left(-\frac{\alpha(x) \Delta z}{2}\right) \exp\left(\frac{i2\pi n(x) \Delta z}{\lambda}\right) A(x, z), \quad (8)$$

where $\alpha(x)$ is the intensity attenuation coefficient and $n(x)$ is the refractive index. The full BPM solution consists in alternating between Eq. (7) (diffraction) and Eq. (8) (modulation). Note that the two effects are concurrent in the actual propagation, but we separate them within our thin slices for tractable calculation. The BPM model will closely approximate the actual solution as the slices are made thin enough.

The phase profile across the beam-steering device is ideally composed of a set of linear phase ramps climbing to 2π OPD and then resetting to zero. We insert this spatially dependent phase profile into the modulate function of the BPM. Phase ramps designed to give 2π resets at λ_{design} are altered at other wavelengths λ_{probe} according to

$$\text{OPD}(x; \lambda_{\text{probe}}) = \frac{\lambda_{\text{design}}}{\lambda_{\text{probe}}} \frac{\Delta n(\lambda_{\text{probe}})}{\Delta n(\lambda_{\text{design}})} \text{OPD}(x; \lambda_{\text{design}}), \quad (9)$$

where the dispersion of Δn in the visible is approximated by

$$\Delta n(\lambda) = G \frac{\lambda^2 \lambda_*^2}{\lambda^2 - \lambda_*^2} \quad (10)$$

with λ entered in nanometers (for E7 we have $G = 3.06 \times 10^{-6}$ and $\lambda_* = 250$ nm).⁶ The phase resets occur at the same transverse locations x , but now the OPD is not necessarily 2π there, so we have diffraction-grating dispersion for wavelengths other than λ_{design} . We found that this simple BPM model of the beam steering device accurately predicts the impulse response throughout the visible.¹³

2.2 Wiener Filtering Algorithm

We model the imaging device as a linear system, so that the steered image is expressed as a linear convolution

$$g(m) = \sum_{l = -\infty}^{\infty} h(m-l) f(l), \quad (11)$$

where $g(m)$ represents the image, $f(l)$ is the object, and $h(m)$ is the point spread function (PSF) of the beam-steering device. The inverse filter^{7,8,14,15} is readily derived by taking the Fourier transform of Eq. (11), yielding

$$H^l(\omega) = \frac{1}{H(\omega)}, \quad (12)$$

which when multiplied by the transform of the degraded image, $G(\omega)$, returns the transform of the object, $F(\omega)$. A simple inverse filter, however, is very sensitive to noise. Since noise cannot be avoided, an alternative filtering method must be employed: the Wiener filter. An estimate $\hat{f}(m)$ of the object $f(m)$ is desired such that the expectation value ($E\{\}$) of the mean squared error,

$$\zeta_e = E\{[f(m) - \hat{f}(m)]^2\}, \quad (13)$$

is minimized. This estimate is given by a convolution of the blurred image with the inverse Fourier transform of the inverse filter $H^l(\omega)$ (given by h^l below):

$$\hat{f}(m) = \sum_{l = -\infty}^{\infty} h^l(m-l) g(l). \quad (14)$$

A more accurate model for this system includes additive noise such that

$$g(m) = \sum_{l = -\infty}^{\infty} h(m-l) f(l) + \eta(m), \quad (15)$$

where $\eta(m)$ is assumed to be a stationary noise sequence uncorrelated with the object $f(l)$. The frequency response of the optimal filter, denoted $H^W(\omega)$, considering an additive noise term is provided by the Fourier Wiener filter⁷

$$H^W(\omega) = \frac{H^*(\omega) S_{ff}(\omega)}{|H(\omega)|^2 S_{ff}(\omega) + S_{\eta\eta}(\omega)} = \frac{1}{H(\omega)} \cdot \frac{|H(\omega)|^2}{|H(\omega)|^2 + S_{\eta\eta}(\omega)/S_{ff}(\omega)}, \quad (16)$$

where S_{ff} and $S_{\eta\eta}$ are the power spectral densities of the object and noise, respectively, and H is the frequency response of the beam steerer. Since it is difficult to estimate the power spectrum of the noise and signal, a constant Γ that represents an average noise-to-signal ratio is often substituted. This simplification gives the form of the Wiener filter used in calculations^{7,8,14,15}:

$$H^W(\omega) \approx \frac{1}{H(\omega)} \cdot \frac{|H(\omega)|^2}{|H(\omega)|^2 + \Gamma} \quad (17)$$

To accommodate effects that contribute to the steering behavior but are not taken into account by the first two steps of our model, we utilize the LMS algorithm. The LMS adapts to specific signal and noise statistics in a training sequence.

2.3 LMS Algorithm

The LMS algorithm applies a finite-impulse-response linear filter to the degraded image and adjusts the filter weights to produce an image that best approximates the desired image under the mean squared error (MSE) criterion.^{8,14,15} Note that the desired response must also be supplied. Therefore, we can only utilize the LMS algorithm when we have the luxury of the appropriate training data. The improved filter can then be used to restore other statistically similar degraded images.

Let us consider the input sequence $\{g(m)\}$ and the desired sequence $\{f(m)\}$ consisting of $N+1$ samples from the detector array. Let $\mathbf{g}(m)$ be an observation vector containing samples spanned by a moving window that passes across the input sequence. Specifically, this vector is denoted

$$\mathbf{g}(m) = [g(m-L) \quad \dots \quad g(m) \quad \dots \quad g(m+L)]^T \quad (18)$$

Note that the steered sequence $\{g(m)\}$ is padded with L zeros at each end. We express the filter output at each position m as the product of the observation vector and the filter weights:

$$\hat{f}(m) = \mathbf{W}^T \mathbf{g}(m) \quad (19)$$

where \mathbf{W} is a $2L+1$ length vector of filter weights. From this expression, the error between the filter output and the desired signal $f(m)$ is

$$\xi(m) = f(m) - \hat{f}(m) = f(m) - \mathbf{W}^T \mathbf{g}(m) \quad (20)$$

Since the MSE ζ_e is a quadratic function of the filter weights [Eq. (13)] with a single fixed minimum point, that point can be readily found using gradient descent techniques.⁸ The gradient descent method adapts the weight vector to seek the minimum MSE and thus give the optimal filter weights. The gradient is found by differentiating the MSE with respect to the filter weights. Assuming the square of the error, ξ^2 , is an estimate of the MSE, a gradient estimate can be found at each position m . Differentiating ξ^2 with respect to the filter weights yields the gradient estimate vector

$$\hat{\nabla}(m) = -2\xi(m)\mathbf{g}(m) \quad (21)$$

The LMS adaptive algorithm uses this estimate of the gradient to adjust the weights according to

$$\mathbf{W}(m+1) = \mathbf{W}(m) + \mu[-\hat{\nabla}(m)] \quad (22)$$

which then reduces to the applicable form⁸

$$\mathbf{W}(m+1) = \mathbf{W}(m) + 2\mu\xi(m)\mathbf{g}(m) \quad (23)$$

where μ regulates the speed and stability of the adaptation process. Using Eq. (23), the LMS algorithm is implemented without squaring, averaging, and differentiation.

The BPM provides an estimate of the beam steerer's finite impulse response (FIR). The discrete Fourier transform of $h(m)$ yields samples of $H(\omega)$, which when used in Eq. (17) give samples of $H^W(\omega)$. We then apply inverse discrete Fourier transformation to find the spatial-domain filter coefficients. These filter coefficients are the initial weights for the LMS algorithm and reduce the adaptation steps necessary to achieve minimum-mean-square error. The LMS algorithm requires a desired and an observed sequence for adapting \mathbf{W} . For the small steer angles studied here, the steered and unsteered images contain common information that is used for the training data. Note that we utilize the steered image as our input sequence and a shifted version of the unsteered image as our desired sequence. We now demonstrate the characteristics and restoration ability of this filter design.

3 Experimental Results

To characterize the beam-steering device, we constructed an imaging system with which we measure both steered and unsteered targets using either narrow- or broadband illumination (Fig. 2). To acquire the narrowband images we use a circular variable interference filter as the spectral filter in the figure. Rotating this filter tunes its passband over the entire visible spectrum with a bandwidth of ± 1 nm. The spectral filter for the broadband images consisted of a low-pass and a high-pass filter, producing a bandpass filter of 400 to 700 nm.

3.1 Narrowband Steering: Experimental Versus Theoretical

Initial measurements were obtained using a 25- μm single-slit target. The steered image of the slit (for a given steer angle and spectral band) approximates the impulse response of the beam-steering device. Figure 3 shows the result of steering 682-nm light with a phase profile designed for steering to 0.024 deg at 543 nm. Figures 3(a) and 3(b) show a single horizontal slice taken out of the original two-dimensional unsteered and steered image, respectively. The steered signal shows grating-order echoes because the phase profile was blazed for 543 nm and not 682 nm. Material dispersion is absent because the radiation is narrowband. The low steering efficiency ($\approx 62\%$) and multiple echoes at this wavelength require the restoration process to place the echoed energy back in the main steered peak.

The LMS filtering algorithm uses the unsteered image as the desired result and minimizes the error between it and the restored image. To make the filter robust, we increase the amount of training data by forming long vectors from multiple 1-D slices of the steered and unsteered images. These vectors represent a larger sample from which the filter coefficients adapt in the presence of statistical variations such as detector nonlinearities and noise. Restored versions of the single slit are presented in Figs. 3(c) and 3(d). The MSE between the Wiener-filter estimate [Fig. 3(d)] and the unsteered image is 1.1×10^{-3} , which is a reduction from the

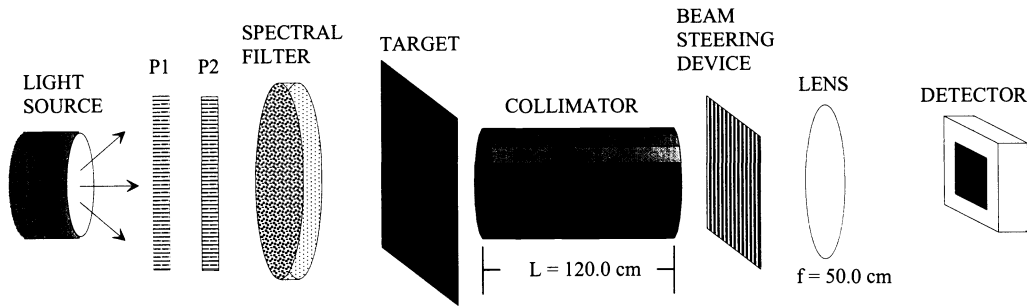


Fig. 2 Imaging system using the broadband beam steerer to steer the field of view. P1 and P2 are sheet polarizers that ensure that the light polarization lies along the director of the liquid crystals and adjust the total transmittance into the detector. The device steers in the horizontal direction.

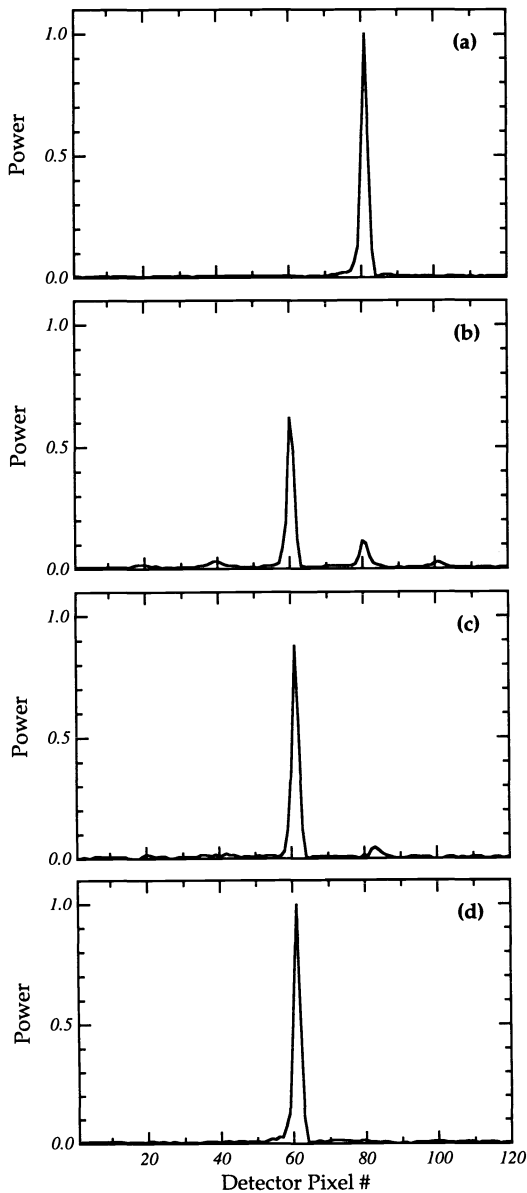


Fig. 3 Narrowband images of 25- μm slit: (a) unsteered, (b) steered, (c) restored with Wiener filter, and (d) restored with LMS filter.

initial MSE (between the steered and unsteered) of 3.9×10^{-3} . The LMS filter gives a better restoration by further reducing the MSE to 9.02×10^{-5} . Figure 4 shows the similarities between the Wiener-filter coefficients derived from the BPM model and the optimal LMS filter found with the experimental training data. The BPM-derived filter gives a good starting point for the LMS algorithm, thus reducing the number of adaptation steps.

To further test our ability to predict the behavior of the beam-steering device, we used the BPM to compute the steering of 682-nm light with phase ramps optimized to steer 543-nm light to different steer angles (0.002 to 0.024 deg).

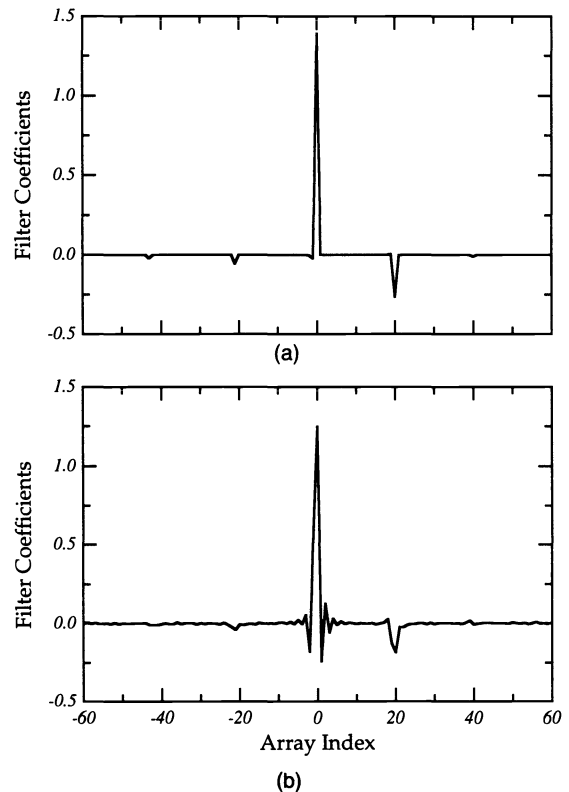


Fig. 4 (a) Wiener-filter impulse response derived from BPM model; (b) LMS optimized filter coefficients for 25- μm slit.

The Wiener-filter coefficients were calculated from the impulse response at each steer angle and then compared with LMS-filter coefficients computed using measured data. Note that the primary features of the filter coefficients displayed in Fig. 4 are a central lobe corresponding to the main steered peak and two negative lobes corresponding to the largest undesired echoes [see Fig. 3(b)]. When we steer to smaller angles, the reset spacing Λ increases and Eq. (4) implies that the angular spacing between grating orders will decrease and thus reduce the peak-to-echo separation in the far field. We therefore expect reduced spacing between the filter peak and each of the two main negative bumps. Figure 5(a) shows excellent agreement between the peak-to-sidelobe separation distance in the BPM-derived Wiener coefficients and the experimentally determined LMS coefficients. If we now measure the sidelobe-to-peak magnitude ratio, we get reasonable agreement between theoretical and experimental results. These results demonstrate the accuracy of the BPM in computing the impulse response of the beam steerer for different phase ramps. The accuracy is similar when we use a single phase ramp (optimized at 543 nm) and probe at different wavelengths.

3.2 Broadband Steering: Filter Generalizability

What will happen when we optimize a restoration filter with an impulse response measured in the lab and then apply this filter to an image acquired in the real world? To test the generalizability of our image restoration filter we acquired images of both a single slit and a military bar target with a broadband (400 to 700 nm) white light source. Since the design wavelength was 543 nm, this passband represents $\approx 20\%$ bandwidth. An optimal filter was calculated from the

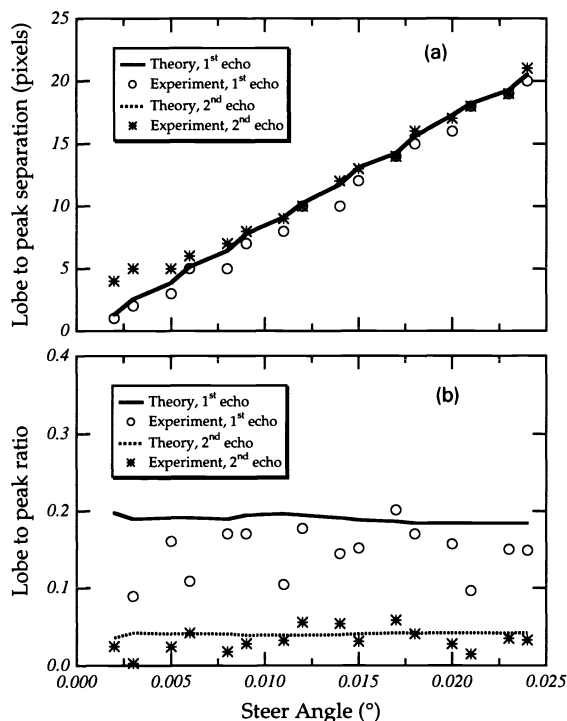


Fig. 5 (a): Peak-to-sidelobe filter coefficient separation in pixels. (b): Sidelobe-to-peak filter coefficient ratio from theoretical predictions and experimental measurements.

steered and unsteered images of the single slit, and this filter was then applied to the steered image of the military bar target. The unsteered, steered, and restored images of the bar target are shown in Fig. 6.

By creating an optimal filter using an approximate impulse response, complicated images can be successfully restored with limited prior knowledge of the original scene. The importance of this discovery becomes obvious when considering the use of the liquid-crystal steering device in a real-world application, where it may be difficult to measure an impulse response in the field or calculate an optimal restoration filter for any given field of view.

As a final demonstration, a steered spoke-target image was restored using LMS filter coefficients derived directly from steered and unsteered image data. Filter coefficients were calculated for two different spoke-target images captured under the same conditions (one as in Fig. 7 and one with higher spoke density). The coefficients for the two targets were found to be nearly identical, thus presenting another example of filter generalizability. The unsteered, steered, and restored images of one spoke target are shown in Fig. 7. The restored image represents a reduction in the MSE from 1.56×10^{-2} to 1.60×10^{-3} .

4 Conclusion

We have demonstrated the image restoration ability of the BPM \rightarrow Wiener filter \rightarrow LMS adaptive filtering algorithm chain. Our procedure successfully removed much of the material and grating dispersion introduced when steering the field of view with a liquid-crystal beam-steering device. We also confirmed the generalizability of the image restoration algorithm with filters derived from impulselike images applied to bar targets. In the ideal case, we can compute a filter based solely on the BPM \rightarrow Wiener filter chain that can then partially restore any image with the corresponding steer angle and wavelength (passband). When we have experimental training data we can further refine our filter with the LMS algorithm. For an operational system we can train our LMS filters with impulse responses measured beforehand and then apply the filters to newly acquired images. Unfortunately, changing the steer angle or wavelength by increments as small as 0.001 deg or 4 nm requires a new filter for successful restoration. A new filter can be readily calculated with BPM, but knowledge of the spectral structure of the image is required. The spectral sensitivity of the restoration process is especially disturbing because the spectral characteristics of the imaged object may be unknown. Future analysis will concentrate on testing the restoration ability of our filters when the imaged scene is spectrally diverse (spectral content varies spatially).

Acknowledgments

We thank Larry Barnes and Al Carney for assistance in capturing the images. We gratefully acknowledge helpful conversations with Ed Watson and Bill Martin, and we thank Paul McManamon and Don Tomlinson for making this research possible. This work was performed under Air Force contract F33601-95-D-J010.

References

1. P. F. McManamon, E. A. Watson, T. A. Dorschner, and L. J. Barnes,

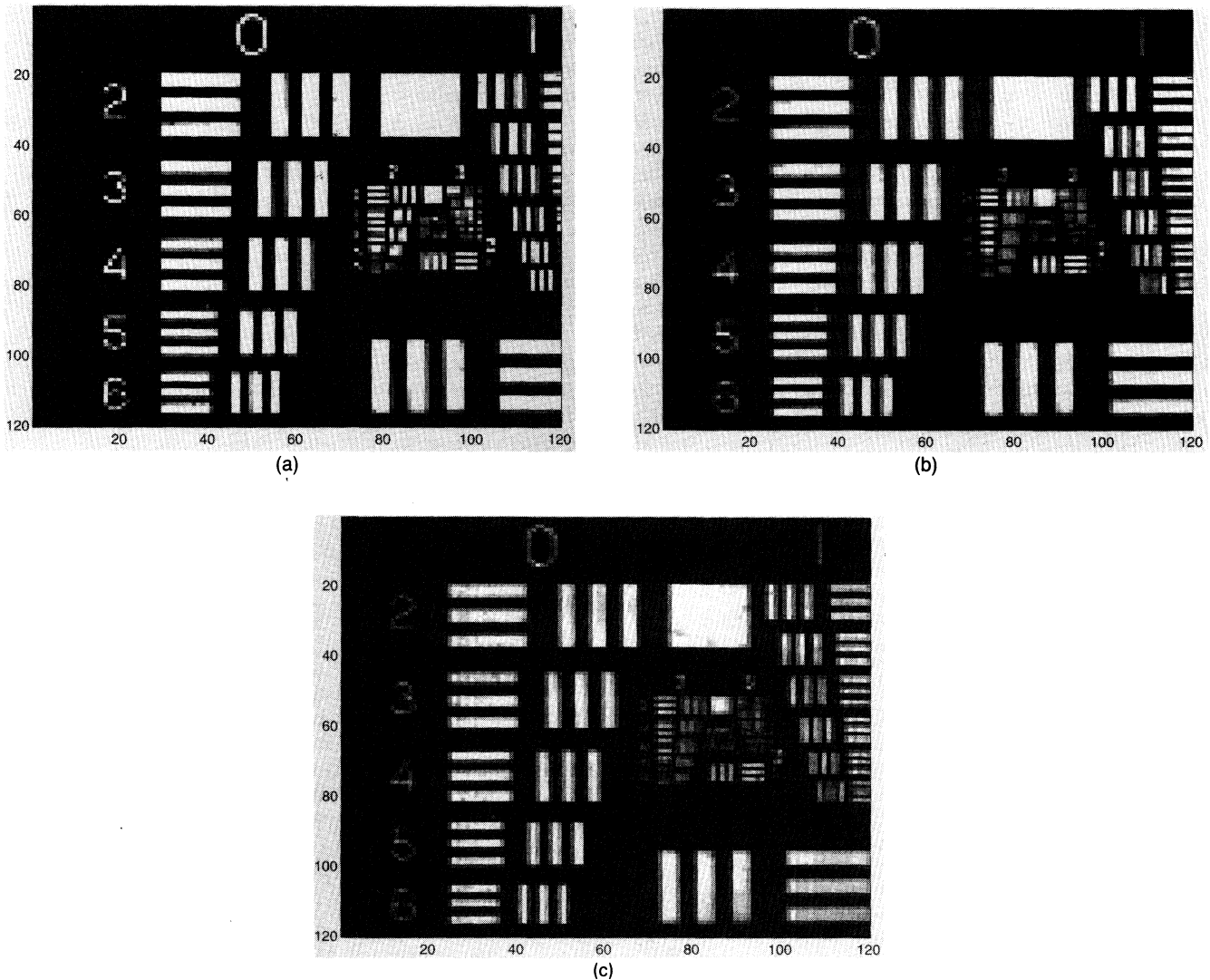


Fig. 6 (a) Unsteered, (b) steered, and (c) restored broadband image of a military bar target. The restoration filter was derived from previously measured single-slit images (not shown). The echoing is significantly reduced.

1. "Applications look at the use of liquid crystal writable gratings for steering passive radiation," *Opt. Eng.* **32**(11), 2657–2664 (1993).
2. P. F. McManamon, E. A. Watson, L. J. Barnes, and A. Carney, "Application of dynamic gratings to broad spectral band beam steering," *Proc. SPIE* **2120**, 178–185 (1994).
3. P. F. McManamon, E. A. Watson, T. A. Dorschner, and L. J. Barnes, "Nonmechanical beam steering for active and passive sensors," *Proc. SPIE* **1969**, 2–10 (1993).
4. K. J. Barnard, E. A. Watson, and P. F. McManamon, "Nonmechanical microscanning using optical space-fed phased arrays," *Opt. Eng.* **33**(9), 3063–3071 (1994).
5. T. C. Cheston and J. Frank, "Phased array radar antennas," Chapter 7 in *Radar Handbook*, M. I. Skolnik, Ed., McGraw-Hill, New York (1990).
6. S.-T. Wu, "Birefringence dispersions of liquid crystals," *Phys. Rev. A* **33**(2), 1270–1274 (1986).
7. A. K. Jain, *Fundamentals of Digital Image Processing*, pp. 267–284, Prentice-Hall, Englewood Cliffs, NJ (1989).
8. B. Widrow and S. D. Stearns, *Adaptive Signal Processing*, pp. 99–114, Prentice-Hall, Englewood Cliffs, NJ (1985).
9. M. D. Feit and J. A. Fleck, Jr., "Light propagation in graded-index optical fibers," *Appl. Opt.* **17**(24), 3990–3998 (15 Dec. 1978).
10. J. A. Fleck, J. R. Morris, and M. D. Feit, "Time-dependent propagation of high energy laser beams through the atmosphere," *Appl. Phys.* **10**, 129–160 (1976).
11. R. Johnson and A. R. Tanguay, Jr., "Optical beam propagation method

- for birefringent phase grating diffraction," *Opt. Eng.* **25**(2), 235–249 (1986).
12. J. Goodman, *Fourier Optics*, pp. 30–50, McGraw-Hill, San Francisco (1968).
13. V. Dominic, A. Carney, and E. A. Watson (unpublished).
14. B. Widrow, J. M. McCool, M. G. Larimore, and C. R. Johnson, Jr., "Stationary and nonstationary learning characteristics of the LMS adaptive filter," *Proc. IEEE* **64**(8), 1151–1162 (Aug. 1976).
15. S. J. Orfanidis, *Optimum Signal Processing: An Introduction*, pp. 278–324, Macmillan, New York (1985).



Ronald J. Broessel received his BS degree in physics from the University of Wisconsin—Eau Claire in 1993. He is presently working towards a MS degree in electro-optics at the University of Dayton in Dayton, Ohio. Current research involves working as a subcontractor for Technology/Scientific Services Inc. (T/SSI) performing research at Wright-Patterson Air Force Base, Ohio. His research interests include adaptive signal and image

processing, nonmechanical beam steering, and liquid-crystal refractive devices.

IMAGE RESTORATION OF DISPERSION-DEGRADED IMAGES

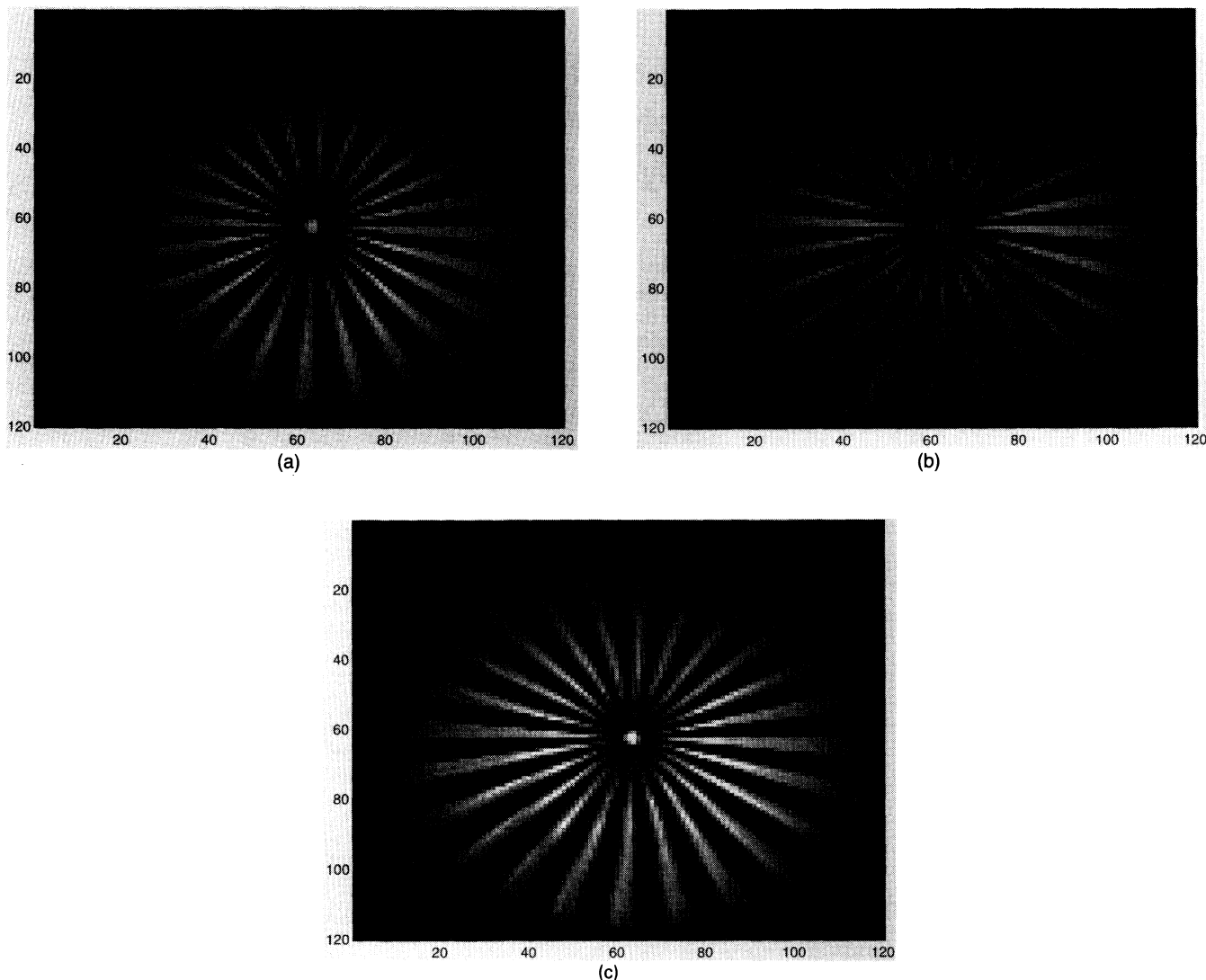
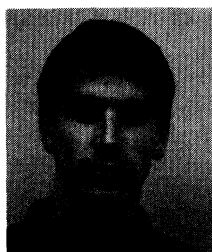


Fig. 7 (a) Unsteered, (b) steered, and (c) restored broadband image of a spoke target. The restoration filter was derived solely from the LMS algorithm.



Vince Dominic graduated in 1986 with a BS degree in electrical engineering from the University of Dayton. He then headed west and earned a PhD from the University of Southern California in 1993. He recently returned to the midwest and joined the Center for Electro-Optics at the University of Dayton. Dr. Dominic's research interests include beam steering, nonlinear optics in fibers and glass, and polymer electro-optic devices.

Russell C. Hardie: Biography and photograph appear with the paper "Aliasing reduction in staring infrared imagers utilizing subpixel techniques" in this issue.